Asian Journal of Chemistry; Vol. 28, No. 9 (2016), 2020-2024

ASIAN JOURNAL OF CHEMISTRY

http://dx.doi.org/10.14233/ajchem.2016.19880

Preparation and Characterization of CeO_2-C_{60} Nanocomposites and Their Application to Photocatalytic Degradation of Organic Dyes

JIULONG LI[1], JEONG WON KO[1] and WEON BAE KO[1,2,*]

[1]Department of Convergence Science, Graduate School, Sahmyook University, Seoul 139-742, Republic of Korea
[2]Department of Chemistry, Sahmyook University, Seoul 139-742, Republic of Korea

*Corresponding author: Fax: +82 2 9795318; Tel: +82 2 33991700; E-mail: kowb@syu.ac.kr

Received: 1 February 2016; *Accepted*: 25 April 2016; *Published online*: 1 June 2016; AJC-17936

Cerium oxide nanoparticles were prepared by the reaction of cerium nitrate hexahydrate and sodium hydroxide. Cetyltrimethyl ammonium bromide ($C_{19}H_{42}NBr$) was added as a templating agent. The yellow precipitate obtained by the reaction was calcined with fullerene (C_{60}) for 2 h at 700 °C in an electric furnace to synthesize CeO_2-C_{60} nanocomposites. The synthesized samples were characterized by X-ray diffraction, scanning electron microscopy. The photocatalytic activity of the CeO_2-C_{60} nanocomposites for the degradation of organic dyes such as methylene blue, brilliant green, rhodamine B and methyl orange upon irradiation with 254 nm UV light was investigated using a UV-visible spectrophotometer.

Keywords: CeO_2-C_{60} nanocomposites, UV irradiation, Photocatalytic activity, Degradation, Organic dyes.

INTRODUCTION

Currently, the synthesis of nanoparticles with desired morphology and characteristic is still a challenging task due to their high-surface area and unique physical, chemical and optical properties [1-4]. Since research on TiO_2 and ZnO nanoparticles was first reported, the investigation of photocatalytic semiconductor catalysts has attracted significant attention from many researchers [5-7]. Consequently, many semiconducting metal oxides such as Fe_2O_3 [8], V_2O_5 [9], Bi_2O_3 [10,11], WO_3 [12,13] and CeO_2 [14] have been synthesized and applied as visible-light-driven photocatalysts.

Among various semiconductor materials, cerium oxide (CeO_2) is a stable rare earth metal oxide that has been studied in many fields for a variety of applications [15,16]. Cerium oxide has a cubic lattice, which means that each Ce^{4+} ion in a unit cell is surrounded by eight O^{2-} ions [17]. Because of the high oxygen storage capacity of CeO_2, oxygen can be transferred between the III and IV oxidation states of cerium in the CeO_2 crystal, which is responsible for its unique properties, such as photocatalytic activity and high stability [18,19] and its use in catalysts, oxygen sensors, hybrid solar cells and electrolytes for solid oxide fuel cells [15,20,21]. Like TiO_2 and ZnO, CeO_2 has attracted the attention of a growing number of researchers as a photocatalyst [22]. In fact, CeO_2 and TiO_2 are similar in many respects. Due to the CeO_2 nanoparticles have large energy band gap of 3.2 eV and long lifetime of photogenerated electron-hole pairs, they have limited photocatalytic activity [23,24]. Therefore, combination of other semiconductors with CeO_2 nanoparticles is a promising method for resolving these problems, because the spectral response range and charge separation can be increased *via* combination [16]. Recently, the transformation of materials into carbon-based materials has been considered an important and effective method for improving the catalytic activity of materials and this method has been applied in many studies [25].

In recent years, with environmental problems becoming more and more serious, many investigations on visible-light-driven semiconductor photocatalysts have been carried out [26,27]. A photocatalytic process using carbon-based metal oxide nanocomposites was found to be an effective technology for wastewater treatment because of its usefulness in cleaning non-biodegradable materials such as organic dyes, aromatic compounds and pesticides in wastewater [28,29]. The photocatalyst creates electron-hole pairs under UV light irradiation to promote the reaction. The photocatalytic activity of nanocomposites is largely determined by the band gap energy for creating electron-hole pairs [5,19]. Compared with the larger band gap of metal oxides, the more appropriate smaller band gap of carbon provides a suitable condition for the transfer of electrons in the reaction and has a positive effect on the photocatalytic activity of the nanocomposites.

Many alternative methods have been used for the preparation of CeO_2 nanoparticles, such as solution precipitation

[30], sol-gel processing [31], a microemulsion procedure [32], thermal decomposition [33], hydrothermal synthesis [4] and use of a self-assembled system [34]. It has also been reported that metal oxide nanoparticles with good thermal stability could be synthesized by using surfactants [35]. In this study, we have fabricated CeO_2 nanoparticles by hydrothermal synthesis and added cetyltrimethyl ammonium bromide (CTAB) as a surfactant. Subsequently, fullerene (C_{60}) and CeO_2 powder were calcined at 700 °C in an electric furnace to obtain the CeO_2-C_{60} nanocomposites. The prepared samples were characterized by X-ray diffraction, scanning electron microscopy and UV-visible spectrophotometry. The photocatalytic activity of CeO_2-C_{60} nanocomposites for the photo-degradation of brilliant green (BG), methyl blue (MB), methyl orange (MO) and rhodamine B (RhB) was evaluated under irradiation with 254 nm UV light.

EXPERIMENTAL

Cerium(III) nitrate hexahydrate [$Ce(NO_3)_3 \cdot 6H_2O$], cetyltrimethyl ammonium bromide ($C_{19}H_{42}BrN$), brilliant green ($C_{27}H_{34}N_2O_4S$) and methyl orange ($C_{14}H_{14}N_3NaO_3S$) were purchased from Sigma-Aldrich (China). Sodium hydroxide, methylene blue $3H_2O$ ($C_{16}H_{18}ClN_3S \cdot 3H_2O$), rhodamine B ($C_{28}H_{31}ClN_2O_3$) and tetrahydrofuran were obtained from Samchun Chemicals (Korea). Fullerene (C_{60}) was supplied by Tokyo Chemical Industry Co., Ltd. All of the chemical materials were used directly without any further purification.

Synthesis of cerium dioxide (CeO_2) and CeO_2-C_{60} nanocomposites: Cerium(III) nitrate hexahydrate and sodium hydroxide were used as the starting reagents to prepare cerium dioxide powder by the precipitation method. Aqueous solutions of [$Ce(NO_3)_3 \cdot 6H_2O$] (0.05 M, 200 mL) and NaOH (0.167 M, 300 mL) were added to an aqueous solution of CTAB (0.025 M, 200 mL). The mixture was reacted under stirring condition for 3 h and the process was controlled at 90 °C. After stirring, the mixed solution was left for 12 h at room temperature. Washing of the precipitate was difficult because of the presence of surfactant; therefore, the precipitate was collected by suction filtration using a Buchner funnel and then washed several times with distilled water (60 °C). Cerium oxide powder was obtained after the precipitate was dried at 80 °C in an oven for 12 h. Subsequently, the pale yellow CeO_2 powder and fullerene (C_{60}) (mass ratio of 2:1) were stirred for 15 min in a tetrahydrofuran solution. The CeO_2-C_{60} nanocomposites were synthesized by heating the mixture of CeO_2 and C_{60} powder in an electric furnace (Ajeon Heating Industry Co., Ltd) at 700 °C for 2 h under an inert atmosphere of argon gas.

Characterization of CeO_2-C_{60} nanocomposites: The crystalline phase of the prepared CeO_2-C_{60} nanocomposites was characterized by powder XRD (Bruker, D8 Advance) with CuK_α radiation (λ = 1.54178 Å) in the 2θ range of 5-90° at a scanning rate of 0.02 s^{-1}. The particle size of the CeO_2-C_{60} nanocomposites can be obtained by analyzing the XRD pattern. The morphology of the CeO_2-C_{60} nanocomposites was examined by SEM (JEOL Ltd, JSM-6510) at an accelerating voltage of 0.5 to 30 kV.

Photocatalytic degradation of organic dyes using the CeO_2-C_{60} nanocomposites: The photocatalytic performances of the synthesized CeO_2-C_{60} nanocomposites were determined by the degradation of organic dyes, such as brilliant green, methylene blue, methyl orange and rhodamine B, under UV light irradiation. The radiation source was a UV lamp (8 W, 254 nm, 77202 Marne La Valee-cedex 1 France). A UV-visible spectro-photometer (Shimadzu UV-1619 PC) with a 200 to 800 nm wavelength range was used to measure the absorbance of the organic dyes. The photocatalytic degradation experiment was carried out as follows: first, the concentration of organic dyes was controlled by measuring the absorbance value is 1.0 at λ_{max}. Then, 5 mg of the CeO_2-C_{60} nanocomposites was dispersed in the reactor with 10 mL of aqueous dye solution. After shaking the suspension, the reactor was placed in a dark environment for 30 min to ensure adsorption-desorption equilibrium before UV light irradiation. Determination of the interval time was 5 min and the optical path length between the reactor and UV lamp was fixed at 1.0 cm.

RESULTS AND DISCUSSION

Characterization of the CeO_2-C_{60} nanocomposites: The crystal phase and structure of the CeO_2-C_{60} nanocomposites were examined by powder XRD.

Fig. 1 shows the XRD patterns of the synthesized CeO_2-C_{60} nanocomposites. As shown in Fig. 1, the diffraction peaks are at 2θ values of 28.3°, 32.7°, 47.1°, 55.9°, 58.4°, 68.9°, 76.7° and 79.4°, which can be indexed to the (111), (200), (220), (311), (222), (400), (331) and (420) facets of the cubic CeO_2 structure, respectively (JCPDS 34-0394) [19, 36]. In Fig. 1, clear peaks of C_{60} itself were not be found. After being combined with the metal, the peak of C_{60} always appeared near 2θ = 27°, which indicates that the peak of C_{60} in the CeO_2-C_{60} nanocomposites may overlap with the 2θ = 28.3° peak of the CeO_2 nanoparticles. The low-intensity diffraction peaks confirmed the low crystallinity of the CeO_2 nanoparticles in the CeO_2-C_{60} nanocomposites, while the broad diffraction peaks of the CeO_2 nanoparticles indicated that the particle size of CeO_2 in the nanocomposites was small [17,28].

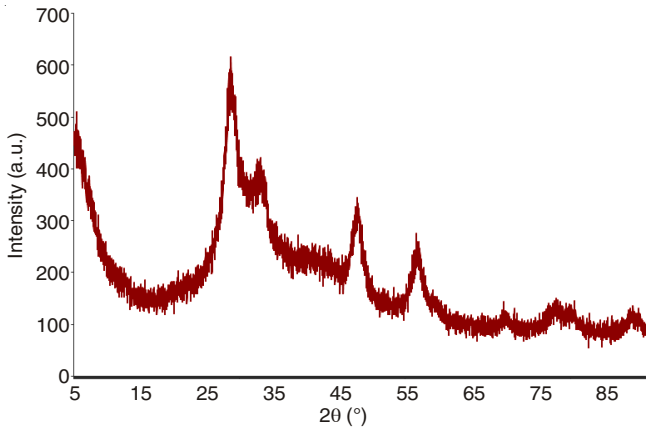

Fig. 1. XRD pattern of CeO_2-C_{60} nanocomposites

The general morphology of the CeO_2-C_{60} nanocomposites was investigated by SEM. Fig. 2 shows the SEM image of the sample. The CeO_2-C_{60} nanocomposites were composed of stone-like C_{60} and rough CeO_2 nanoparticles. Stone-like C_{60} was dispersed in the image and had a large morphological

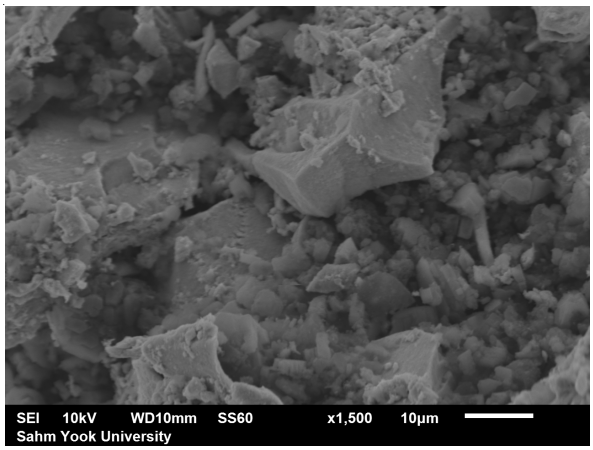

Fig. 2. SEM image of CeO_2-C_{60} nanocomposites

size. The CeO_2 nanoparticles presented a mixed morphology, comprising both crushed stone- and rod-like shapes. The small CeO_2 nanoparticles filled the spaces between the stone-like C_{60} and some particles were attached on the surface of C_{60}.

Photocatalytic degradation of organic dyes: The photocatalytic activities of the CeO_2-C_{60} nanocomposites were evaluated by performing the degradation of brilliant green, methylene blue, methyl orange and rhodamine B under 254 nm UV light irradiation.

Fig. 3 shows the UV-visible spectra for the degradation of (a) brilliant green, (b) methylene blue, (c) methyl orange and (d) rhodamine B in the presence of the CeO_2-C_{60} nanocomposites as a photocatalyst. It was reported that the catalyst redox activities of metal oxides could be improved by forming composites [16]. For this purpose, C_{60} was associated with CeO_2 in this study and the concentration of the CeO_2-C_{60} nanocomposites was 0.5 g/L. In order to obtain the adsorption-desorption equilibrium between the CeO_2-C_{60} nanocomposites and organic dyes, the concentration of organic dyes was evaluated after storing in the dark for 30 min. As the irradiation time increased, the colour of the organic dye solution became light, which corresponded with the decrease in the main absorption peaks of the organic dyes in the UV-visible spectra. The schematic of the photo-degradation mechanism for the CeO_2-C_{60} nanocomposites and charge transfer in the nanocomposites is shown in Fig. 4.

Under ultraviolet irradiation, the photoexcited electron (e^-) in the valence band of the CeO_2 crystallite jumped to the conduction band, forming holes (h^+) in the valence band. An identical charge transfer occurred in the C_{60} crystallite. Due to the discrepancy of the band gap energy between the CeO_2 and C_{60} crystallites, the photogenerated electron-hole pairs can be transferred within the nanocomposites. The electrons on the conduction band of the C_{60} crystallite were transferred to the

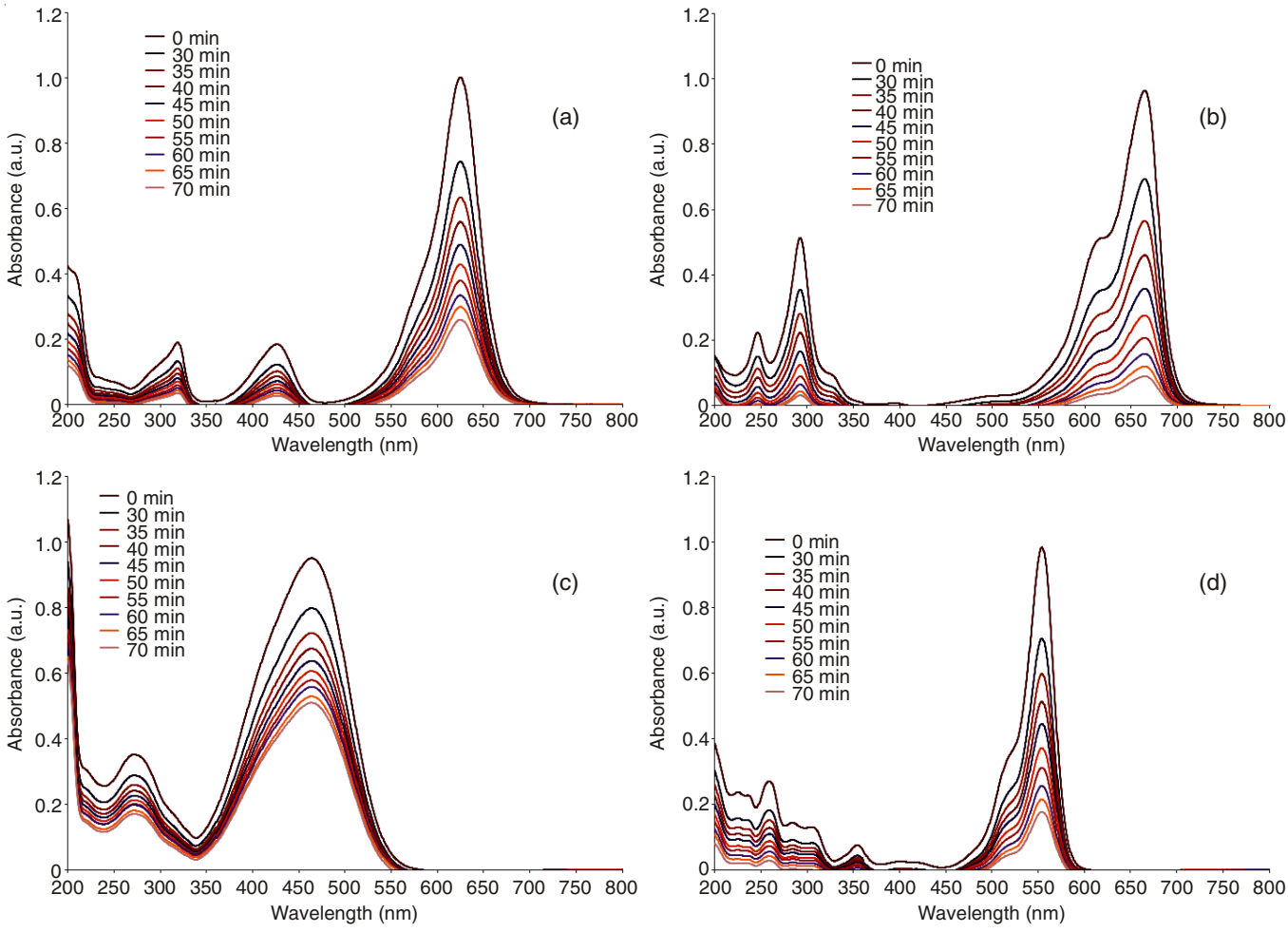

Fig. 3. UV-visible spectra of the degradation of (a) brilliant green, (b) methylene blue, (c) methyl orange and (d) rhodamine B with the CeO_2-C_{60} nanocomposites as a photocatalyst under ultraviolet irradiation at 254 nm

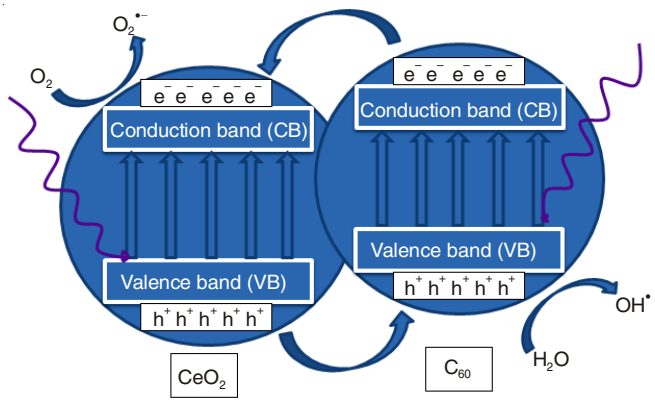

Fig. 4. Charge transfer between CeO_2-C_{60} nanocomposites and photocatalytic degradation mechanisms of organic dyes in the presence of CeO_2-C_{60} nanocomposites

conduction band of the CeO_2 crystallite, the holes on the valence band of the CeO_2 crystallite were transferred to the valence band of the C_{60} crystallite. Photoexcited electrons with strong oxidizing character and photogenerated holes with strong reducing character formed a redox system. Hydroxyl radicals ($OH^{\bullet}$) were produced because of the holes on the valence band in oxidized water (H_2O). Meanwhile, oxygen dissolved in the organic dyes solution was reduced to superoxide anion radicals ($O_2^{\bullet-}$) by the photoexcited electrons on the conduction band. Finally, the generated hydroxyl radicals ($OH^{\bullet}$) and superoxide anion radicals ($O_2^{\bullet-}$) could act as effective oxidizing agents for degrading the organic dyes [16,17,26].

Kinetics study of the CeO_2-C_{60} nanocomposites: To further investigate the photocatalytic efficiency, a kinetics study was performed using the Langmuir-Hinshelwood kinetic model [37].

Fig. 5 illustrates the photocatalytic efficiency of the CeO_2-C_{60} nanocomposites for brilliant green, methylene blue, methyl orange and rhodamine B. The photo-degradation of organic dyes with CeO_2-C_{60} nanocomposites as the photocatalyst followed pseudo-first-order reaction kinetics and the equation can be represented as follows:

$$\ln\left(C/C_0\right) = -K \cdot t$$

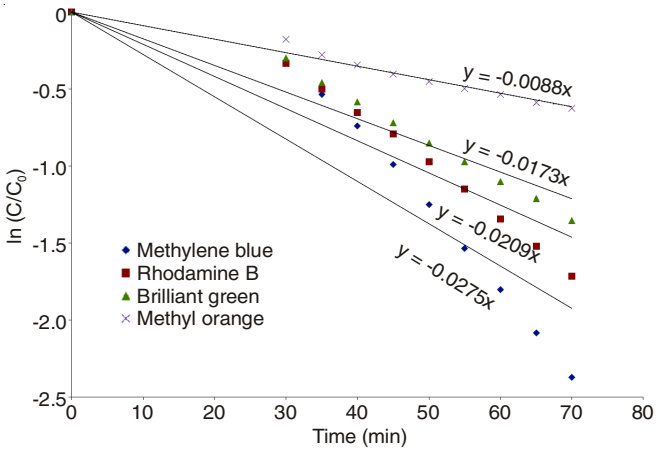

Fig. 5. Kinetics study of the photocatalytic degradation of the organic dyes using CeO_2-C_{60} nanocomposites as a photocatalyst

here, C is the concentration of organic dyes at irradiation time t and C_0 is the initial concentration. K is the rate constant, which can be calculated from the slope. Kinetics study of the photocatalytic degradation of organic dyes indicated that the photocatalytic efficiency order of the CeO_2-C_{60} nanocomposites was methylene blue > rhodamine B > brilliant green > methyl orange.

Conclusion

CeO_2-C_{60} nanocomposites were successfully prepared by hydrothermal synthesis and calcination. The structural and morphological properties of the CeO_2-C_{60} nanocomposites were characterized by XRD and SEM. The analysis results revealed that the fabricated CeO_2-C_{60} nanocomposites have stone-like C_{60} and rough CeO_2 nanoparticles. The CeO_2 nanoparticles exhibited a rough mixed morphology. Moreover, the photocatalytic activity of CeO_2-C_{60} nanocomposites was determined by the degradation of organic dyes under UV light irradiation. Because of composite formation, enhanced electron-hole pairs were produced, which induced the formation of a large amount of hydroxyl radicals ($OH^{\bullet}$) and superoxide anion radicals ($O_2^{\bullet-}$); these radicals played a role in the degradation of the organic dyes. Further, the photocatalytic degradations of organic dyes were shown to follow pseudo-first-order reaction kinetics. By comparing the efficiencies for the photocatalytic degradation of brilliant green, methylene blue, methyl orange and rhodamine B under UV light irradiation at 254 nm, it was determined that the degradation rate of the CeO_2-C_{60} nanocomposites was fastest for methylene blue.

ACKNOWLEDGEMENTS

This study was supported by Sahmyook University research funding in Korea.

REFERENCES

1. J. Malleshappa, H. Nagabhushana, S.C. Sharma, Y.S. Vidya, K.S. Anantharaju, S.C. Prashantha, B.D. Prasad, H.R. Naika, K. Lingaraju and B.S. Surendra, *Spectrochim. Acta A*, **149**, 452 (2015).
2. G.Z. Chen, F.F. Zhu, X. Sun, S.X. Sun and R. Chen, *Cryst. Eng. Comm.*, **13**, 2904 (2011).
3. Y.S. Vidya, K. Gurushantha, H. Nagabhushana, S.C. Sharma, K.S. Anantharaju, C. Shivakumara, D. Suresh, H.P. Nagaswarupa, S.C. Prashantha and M.R. Anilkumar, *J. Alloys Comp.*, **622**, 86 (2015).
4. A.I.Y. Tok, F.Y.C. Boey, Z. Dong and X.L. Sun, *J. Mater. Process. Technol.*, **190**, 217 (2007).
5. V. Klochkov, *J. Photochem. Photobiol. Chem.*, **310**, 128 (2015).
6. J.H. Mo, Y.P. Zhang, Q.J. Xu, J.J. Lamson and R.Y. Zhao, *Atmos. Environ.*, **43**, 2229 (2009).
7. F.B. Li, X.Z. Li, M.F. Hou, K.W. Cheah and W.C.H. Choy, *Appl. Catal. A*, **285**, 181 (2005).
8. H. Xie, Y. Li, S. Jin, J. Han and X. Zhao, *J. Phys. Chem. C*, **114**, 9706 (2010).
9. M. Aslam, I.M.I. Ismail, N. Salah, S. Chandrasekaran, M.T. Qamar and A. Hameed, *J. Hazard. Mater.*, **286**, 127 (2015).
10. A. Hameed, M. Aslam, I.M.I. Ismail, N. Salah and P. Fornasiero, *Appl. Catal. B*, **163**, 444 (2015).
11. T. Saison, N. Chemin, C. Chaneac, O. Durupthy, V. Ruaux, L. Mariey, F. Mauge, P. Beaunier and J.P. Jolivet, *J. Phys. Chem. C*, **115**, 5657 (2011).
12. M. Aslam, I.M.I. Ismail, S. Chandrasekaran and A. Hameed, *J. Hazard. Mater.*, **276**, 120 (2014).
13. T. Arai, M. Yanagida, Y. Konishi, A. Ikura, Y. Iwasaki, H. Sugihara and K. Sayama, *Appl. Catal. B*, **84**, 42 (2008).
14. L.E. Barton, M. Auffan, L. Olivi, J.Y. Bottero and M.R. Wiesner, *Environ. Pollut.*, **203**, 122 (2015).

15. H. Balavi, S. Samadanian-Isfahani, M. Mehrabani-Zeinabad and M. Edrissi, *Powder Technol.*, **249**, 549 (2013).
16. N.S. Arul, D. Mangalaraj and T.W. Kim, *Appl. Surf. Sci.*, **349**, 459 (2015).
17. A. Umar, R. Kumar, M.S. Akhtar, G. Kumar and S.H. Kim, *J. Colloid Interf. Sci.*, **454**, 61 (2015).
18. J. Zhang, B. Wang, H. Cui, C. Li, J.P. Zhai and Q. Li, *J. Rare Earths*, **32**, 1120 (2014).
19. L.N. Wu, S.M. Fang, L. Ge, C.C. Han, P. Qiu and Y.J. Xin, *J. Hazard. Mater.*, **300**, 93 (2015).
20. L.H. Yu and J.Y. Xi, *Int. J. Hydrogen Energy*, **37**, 15938 (2012).
21. T. Desaunay, A. Ringuede, M. Cassir, F. Labat and C. Adamo, *Surf. Sci.*, **606**, 305 (2012).
22. M. Aslam, M.T. Qamar, M.T. Soomro, I.M.I. Ismail, N. Salah, T. Almeelbi, M.A. Gondal and A. Hameed, *Appl. Catal. B*, **180**, 391 (2016).
23. M.A. Lazar, S. Varghese and S.S. Nair, *Catalysts*, **2**, 572 (2012).
24. A. Corma, P. Atienzar, H. Garcia and J.-Y. Chane-Ching, *Nat. Mater.*, **3**, 394 (2004).
25. N. Wang, H. Fan and S.Y. Ai, *Chem. Eng. J.*, **260**, 785 (2015).
26. J. Xu, W.Z. Wang, J. Wang and Y.J. Liang, *Appl. Surf. Sci.*, **349**, 529 (2015).
27. H. Zhao, G.M. Zhang, S. Chong, N. Zhang and Y.C. Liu, *Ultrason. Sonochem.*, **27**, 474 (2015).
28. J. Chaisorn, K. Wetchakun, S. Phanichphant and N. Wetchakun, *Mater. Lett.*, **160**, 75 (2015).
29. J.S. Lee, K.H. You and C.B. Park, *Adv. Mater.*, **24**, 1084 (2012).
30. E.L. Foletto, S. Battiston, G.C. Collazzo, M.M. Bassaco and M.A. Mazutti, *Water Air Soil Pollut.*, **223**, 5773 (2012).
31. T. Yu, Y. Park, M.C. Kang, J. Joo, J.K. Park, H.Y. Won, J. Kim and T. Hyeon, *Eur. J. Inorg. Chem.*, **2008**, 855 (2008).
32. K. Nagy and I. Dekany, *Colloids Surf. A*, **345**, 31 (2009).
33. M.A. Gabal, S.A.K. Elroby and A.Y. Obaid, *Powder Technol.*, **229**, 112 (2012).
34. A. Bumajdad, J. Eastoe and A. Mathew, *Adv. Colloid Interface Sci.*, **147-148**, 56 (2009).
35. Y.J. Wang, J.M. Ma, M.F. Luo, P. Fang and M. He, *J. Rare Earths*, **25**, 58 (2007).
36. M.M. Khan, S.A. Ansari, M.O. Ansari, B.K. Min, J. Lee and M.H. Cho, *J. Phys. Chem. C*, **118**, 9477 (2014).
37. S.K. Kansal, G. Kaur and S. Singh, *React. Kinet. Catal. Lett.*, **98**, 177 (2009).